Flow Visualization and Solute Transport in Evaporating Droplets

Pallippadan Johny Jaijus and Anugrah Singh
Dept. of Chemical Engineering, Indian Institute of Technology Guwahati, Guwahati 781039, India

DOI 10.1002/aic.12096
Published online October 22, 2009 in Wiley InterScience (www.interscience.wiley.com).

We have investigated the velocity field and associated particle transport in an evaporating water droplet using the tool of particle image velocimetry. Experiments were performed where single droplets containing polystyrene particles were exposed to evaporation. Our method applicable to droplets confined between two parallel surfaces differs from the conventional PIV techniques on the 3D droplets and removes many of the limitations associated with mapping of velocity field. To avoid refraction of light at the droplet surface we have studied the motion in a disc-shaped droplet which was prepared by confining the drop between two nonwetting surfaces and its base is pinned to a wetting surface. Experiments were carried out under the conditions where Marangoni flow creates convection cells and finally leading to deposition of particles toward the pinned edge. The contact angle, height of the droplet, velocity field, and the particle concentration inside the evaporating droplet was measured and its time evolution was recorded. © 2009 American Institute of Chemical Engineers *AIChE J,* 56: 1674–1683, 2010
Keywords: evaporation, fluid mechanics, transport, particulate flows, microfluidics

Introduction

We encounter droplet evaporation in everyday life. For example, when a droplet of coffee or any colloidal solution is dropped onto a surface and the droplet dries out, a ring of coffee or the corresponding solute particles is left on the surface. This phenomenon exists not only in everyday life, but also in many practical industrial applications such as spray coating and printing. Ring formation in an evaporating sessile drop is a hydrodynamic process in which particles dispersed in the drop are advected to the contact line and towards the end of evaporation a ring-shaped deposit consisting of solute particles is left on the substrate. Though it appears to be a simple phenomenon, many aspects of microscale such as, Marangoni effects, contact angles with solid substrates, and flow profiles are not yet completely understood. In an evaporating droplet, the knowledge of flow profile is the key to understanding the pattern formation. Because of the small time and spatial scales of the evaporation the measurement of local velocity and concentration fields are not easily accessible experimentally.

Ring-like deposition patterns in drying droplets of colloidal particles have been the subject of study in many experimental investigations. The complete experimental analysis on the coffee drop deposits was conducted by Deegan et al.[1–3] They reported extensive experimental results on the ring formation and demonstrated that these could be quantitatively accounted for. They have also proposed a theory of solute transport in evaporating droplets which is based on capillary flow due to contact line pinning, without considering the convective flow resulting from the temperature gradient within the drop. Theoretical study of the particle deposition during sessile drop evaporation were also performed by Popov[4] and Fischer[5] considering a very thin drop. They derived a height averaged radial velocity and neglected the vertical flow in the drop. Widjaja and Harris[6] have studied particle deposition during sessile drop evaporation through numerical simulations. The vapor concentration profile around the drop, the drop shape, the fluid velocity and pressure, and the particle concentration profile inside the drop have been solved simultaneously. The particle deposition profile is found to be influenced by the convective and

Correspondence concerning this article should be addressed to A. Singh at anugrah@iitg.ernet.in.

diffusive mass transfer of the particles in the bulk liquid and by the deposition rate along the substrate. Hu and Larson developed approximate analytical forms for the evaporation flux and temperature profiles along the droplet surface.[7,8] Subsequently, the effect of Marangoni stresses on the flow in an evaporating sessile drop was studied by them using lubrication analysis and a finite element solution of the flow field in the drying droplet was obtained.[9]

In many experimental studies, it has been shown that convection can occur even for small droplets. The recent experimental results by Hu and Larson[10] indicate that particle deposition in octane droplets can be localized predominantly at the centre of the droplet instead of at the contact line. They have reasoned that the temperature gradient between the apex and the contact line of the droplet generates a nonuniform surface tension on the interface. When the droplet surface is warmer, the surface tension there is smaller than near the substrate and hence drives out the fluid from the inside toward the surface. Because of viscous forces, interface Marangoni motion drags the adjacent fluid layers to the top of the droplet and yields convective motion inside the droplet. Then, the solute particles are predominantly carried by the bulk motion and accumulate near the edge of the droplet. Pearson[11] has shown that the surface tension forces can induce cellular motion in those cases where the criteria given in terms of buoyancy forces would not allow instability. In case of aqueous droplets, if there are surfactants present, they can create conditions that favor thermal Marangoni convection, which otherwise do not occur in aqueous systems.[12] Many studies on pattern formation with droplet evaporation have considered the cases where the contact lined is pinned. Adachi et al.[13] have observed that under certain conditions the competition between the friction force and surface tensions produces ''stick-slip'' motion at the contact line, and hence, the droplet oscillates as it dries and generates a stripped film composed of particles.

Quantitative visualization of fluid flow in an evaporating droplet is of great interest as this phenomenon is fundamental in a large variety of practical applications and scientific researches. This is also of interest to chemist, physicist, chemical, and mechanical engineers to explore wide range of interesting phenomena where patterns of the internal circulation flow in evaporating droplets are believed to play a key role. The knowledge of the flow pattern in an evaporating liquid droplet has many practically important applications and is also of considerable academic interest. The fluid flow inside a droplet plays an important role in the overall transport process. Accurate flow field data are necessary to correlate the hydrodynamic characteristics with the physiochemical processes occurring inside a droplet. Particle accumulation phenomena is also closely related to the flow pattern inside a droplet which is related to the Marangoni force and Marangoni convection (generated by surface tension gradient), near the three phase contact line of air, liquid, and solid. The flow instabilities within the evaporating droplet can produce irregular structures which is influenced by convection pattern and fingering instabilities.[14,15] In recent years, pattern formation in confined geometry has received much attention due to its practical implications in microfluidic devices. Abkarian et al.[16] have studied colloidal crystallization in capillary tubes and observed ring patterns along the length of the tube for different particle concentrations. When a drop of solution containing nonvolatile solute is allowed to evaporate from a capillary bridge between a curved and flat surface, patterns of remarkably high fidelity and regularity are observed.[17,18] Using this approach Xu et al.[19] have shown that nanoparticles can be self-assembled into spatially ordered, 2D patterns by simply allowing a drop of a nanoparticle solution to evaporate from a ''sphere-on-flat'' geometry. Evaporative self-assembly of polymer solution from a sessile drop has emerged as an important surface-patterning technique which has potential application in optical, microelectronic, and sensory devices.[20] Hong et al.[21] were able to get ordered mesoscale polymer patterns of concentric ring and punch-hole-like shape by mediating the interfacial interactions between the polymer and the substrate. It is also possible to get variety of complex and well-ordered structures through controlled evaporative self-assembly of polymer solution by simply changing the upper surface of the imposed geometry.[22] However, control of evaporation process (such as evaporation flux, solute transport, and interaction between solute and substrate) still remains a challenge. It is also desired to have a quick and reliable method to map the flow patterns inside evaporating droplet which can help to understand the solute transport, so that highly ordered structures on a large scale can be produced rapidly and economically.

There are significant experimental and theoretical works performed to investigate various surface tension driven (Marangoni) motion in general flows, but there are only a few reported works studying the flow profile and solute concentration in an evaporating droplet. Zhang and Yang[23] experimentally studied the natural convection in evaporating drops, where they observed a Marangoni flow. Savino and Monti[24] numerically solved the axisymmetric steady state Navier-Stokes equations taking into account the Marangoni stress at the liquid-air interface. They also performed experiments to map the velocity field but their theoretical results were not consistent with the experimental ones due to the errors in using the PIV technique to map the velocity field in a spherical cap droplet which acts like a lens distorting the real flow field. Particle image velocimetry (PIV) is an invaluable tool for flow visualization. However, the refraction of light at the droplet surface makes it difficult to measure flow field inside the droplet accurately. Though there are several problems encountered in finding the velocity field, one of the most significant problems is the image distortion due to the refraction of light at the droplet surface. Without proper correction an accurate quantitative analysis of the internal flow is extremely difficult. This problem was overcome by Kang et al.[25] who have devised ray tracing method with image mapping and velocity mapping method to visualize the natural convection inside an axi-symmetric droplet. In their study it was observed that velocity mapping method is suitable over image mapping method to resolve the image distortion encountered during the flow analysis of the droplet. However, even the velocity mapping method can produce error if the angle between image plane and object plane are not correctly determined. In a recent work, Minor et al.[26] have reported that the ray tracing algorithm by Kang et al. is valid only for hemispherical shapes and needs correction for more general situation of droplets that have shapes closer to that of a sphere with heights much larger than their contact line

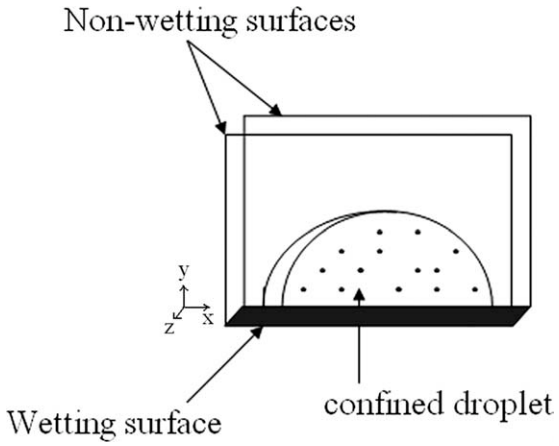

Figure 1. Schematic of arrangement used to make the disc-shaped drop confined between two parallel nonwetting surfaces.

radii. The corrected algorithm with its application is presented in their work. The technique of Pereira et al.[27] using defocusing digital particle image velocimetry is very promising for 3D flow mapping in situations where Marangoni instabilities can produce complex flow patterns inside the evaporating droplets. Recently, Ueno and Kochiya[28] have used 3D Particle tracking method to analyze the spatio-temporal particle motion to study the capillary-driven flow in evaporating droplets. In 3D visualizations, the illumination of the droplet was perpendicular to the substrate surface and images were captured from underneath the transparent surface, which avoided image distortion due to droplet surface reflection. However, planar two-component PIV technique which uses thin light sheet for visualization cannot be used with bottom viewing because, in an axi-symmetric sessile droplets the visualization of the flow field in a plane perpendicular to the base is required. Besides, this restricts the study to transparent substrates only. These methods also require two CCD cameras. The fluorescent flow markers are illuminated with laser source. Each camera provides particle images in 2D plane which is then recombined using pattern matching algorithm to obtain 3D flow field. The defocusing digital particle image velocimetry (DDPIV) recovers the depth coordinate by calculating the separation between defocused images generated by an aperture mask with a plurality of pinholes.[27] In 3D PTV method, the particle motions in successively captured 2D images by each CCD camera are tracked by applying the triple pattern-matching algorithm.[28] In principle, these techniques can be applied to gather whole field velocity information, and are most suitable to study full three-dimensional motion inside evaporating droplets. Though accurate, these techniques and facilities may be out of reach to nonspecialists. Moreover, the aforementioned implementations always have calibration challenges that give severe difficulties in obtaining reliable information.

Here, we provide a simple method to obtain flow field in evaporating droplets which requires less experimental effort. Our method does not require either of the velocity mapping or image mapping as we study the evaporation and solute transport in a drop confined between two parallel plates with narrow gap, thus approximating the 2D flow. This increases the evaporation time but is expected to have no qualitative effect on velocity or concentration field. Thus, we use 2D system as an analog of 3D problem of drying drops with dispersed solids which is of widespread interest. This presents a number of unique advantages such as simplicity of instruments and ease of implementation. By using an objective lens of higher magnification and smaller tracer particles, the system can be extended to submicron flow visualization. No special optical arrangements are required and the particles can be visualized with any light source. Moreover, in this way we were able to obtain simultaneous measurements of velocity and concentration fields. The dynamic contact angles are easily obtained from the 2D photographs. Though, 3D droplet evaporation is more common but there are some applications where liquid droplet evaporation is confined between two surfaces such as DNA array hybridization where the sample is sandwiched in a closed array system made of glass surfaces. The evaporation of the liquid generates forces which uniformly pulls the coiled DNA chains to a straight manner. DNA stretching through droplet drying is able to produce elongated samples without modifying the biochemical properties, where patterns of the internal circulation flow are believed to play a key role.[29,30] In protein crystallography, two-dimensional crystals are assembled by using evaporation-driven convection.[24,31,32]

Experimental Details

Experimental setup

Figure 1 shows the schematic of the arrangement used to generate a disc-shaped droplet. A microslide of 1.1 mm thickness with thin film of paraffin wax coated on it was taken. Another microslide of same thickness with clean surface was placed on it laterally. A small tiny droplet using the micropipette was placed such that it was at the corner of wetting and nonwetting surfaces. Another slide which also had its surface coated with paraffin wax was placed on the top of the droplet. This resulted into a disc-shaped drop confined between two nonwetting slippery surfaces with its contact line pinned on a wetting and rough surface. Because of coating with the paraffin the actual separation between the glass slides was slightly reduced and the thickness of the droplet was measured to be 800 μm. This was found out by taking the side view image of the drop. The diameter of the confined droplet was measured to be 4.45 mm. The assembly was clamped and held on a vertical stand for flow visualization with a camera placed horizontally. Figure 2 shows the

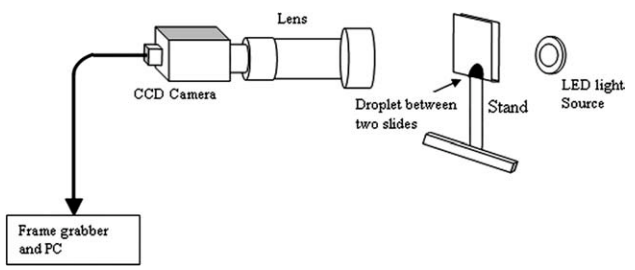

Figure 2. Experimental setup used to carry out PIV studies on evaporating droplets.

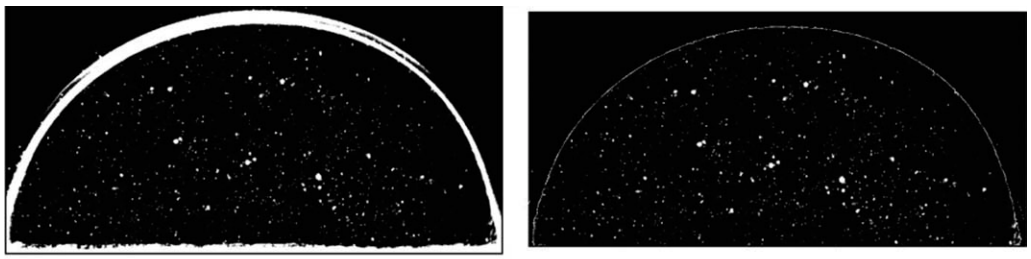

(a) (b)

Figure 3. (a) A sample image of the dispersed particles in an evaporating droplet; (b) cleaned image used for PIV analysis.

schematic of our PIV setup. The droplet with the dispersed latex particles was imaged using a 1360 × 1024 pixels CCD camera (Pixelfly Hires from PCO) in conjugation with a macrozoom lens (Navitar). This camera also allows acquiring images at lower resolution (680 × 512 pixels) at which greater number of images can be stored. A white LED light source was used to illuminate the droplet. This arrangement insured that the effect of refraction from the edge of the droplet is minimized. The images from CCD camera were stored on the computer via frame-grabber card. As the image plane coincided with the velocity plane, there was no need for velocity mapping as required in the visualization of 3D droplets. The images were subsequently analyzed for velocity and concentration fields as described later.

Materials and methods

The particles used in water droplet were white spherical latex particles (Polysciences) of mean diameter 10 μm. First, the particles are dispersed in water with gentle mixing in a beaker. We have used ultra pure water from a Milli-Q system. The suspension was kept for few hours to allow any heavier particles or impurities to settle down. The top portion of the dispersion is then transferred to another beaker. This is used as the sample for the analysis. In the present analysis, we have used 1% (Volume by Volume) of dispersed particles. The experiments were carried out at room temperature of 23°C and the relative humidity was measured to be 60%.

Particle image velocimetry

Particle image velocimetry (PIV) is a nonintrusive, full field optical measuring technique. PIV is used to obtain velocity information about fluid motion and has been applied to a many kinds of flows. In traditional PIV experiments, the fluid of interest is seeded with tracer particles, which are illuminated by a sheet of bright light. The positions of these particles at different times are recorded on a camera and the image sequence is digitized. Particle distance between two successive images ascertains the motion of the fluid. In multiframe/single exposure PIV,[33] two images revealing the positions of tracer particles within the fluid are taken at short time, Δt apart. As it is not possible to track individual particles, so a statistical analysis is required. Each image is divided into a grid of small sections called as interrogation areas. The corresponding interrogation areas within each of the two images are then cross-correlated. The cross-correlation function is effectively a pattern matching routine that determines which displacement is required to shift the first area to best overlap the second area. By scaling this area by the magnification of the camera lens and dividing by Δt, the average velocity for the fluid within the interrogation area is obtained. This process is repeated at each grid point within the image, resulting in a map of velocity vectors to describe the flow.

Acquisition of PIV images

The optical system for PIV experiments is sketched in Figure 2. A single drop of water containing the solute particles was placed on the wetting surface confined between two wax-coated nonwetting surfaces. The droplet takes the shape of a disc whose base is pinned to the substrate and the other two confining parallel surfaces are unpinned. The images were taken using CCD camera placed perpendicular to the plane of the drop and the time of evaporation was also noted down. The camera is operated in video mode to capture images at 19 frames/s. The images were taken in the presence of white LED light source. The CCD camera is connected to a computer where the images are recorded in 12 bit format gray images. Because of limited memory size of the frame grabber card a set of 100 images is taken at a time and transferred to the computer. The procedure is repeated till the images showed no significant number of dispersed particles. Figure 3a shows a sample PIV image of the droplet and solute particles. There was small refraction from the top surface as well as base of the droplet and the image shows bright regions there. In the PIV analysis, the images were first cleaned using an edge detection program to remove the white pixels from the edge as well as base of the droplet as shown in Figure 3b. The cleaned image used for particle count is estimated to have about 8% less particles due to removal of the boundary region. However, this is not expected to affect the qualitative analysis of the particle dynamics.

Interrogation of PIV photographs

The digitized photographs were saved in 680 × 512 pixels, 12 bits format gray scale images on a computer via frame grabber. To calculate the velocity from pair of images we have used the PIV analysis software PIV SLEUTH.[34] The image pairs were interrogated using two-frame cross

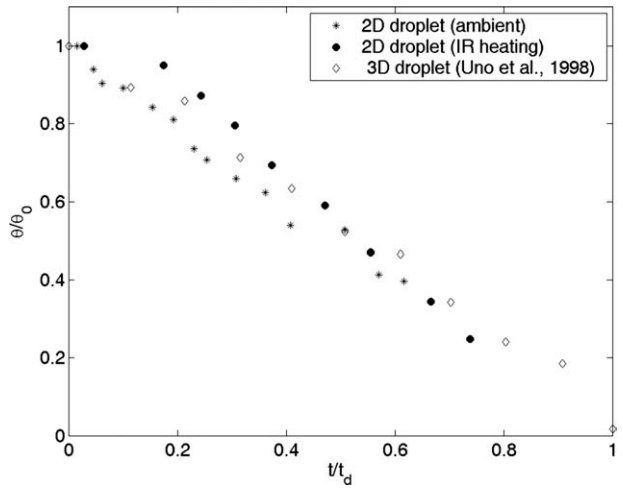

Figure 4. Time evolution of contact angle (θ) for confined 2D droplet and 3D droplet;[35] θ_o is the initial contact angle and t_d is the total drying time.

correlation technique of Adrian et al.[33] Two-frame cross correlation is a highly accurate method. In this method, the pair of images is imaged onto separate frames. Such correlation gives only a single displacement peak and hence is ideal for flows that have flow reversal and vortical structures. Unlike autocorrelation or one-frame cross-correlation it does not require information about the mean flow direction. In our experiments, the time difference between two images was 52 ms. The spot size in the earlier stage of evaporation for flow field interrogation was 64 × 64 pixels with 75% overlap between interrogation spots. This gives us velocity vectors which are spaced 0.105 mm apart. In the later stages of evaporation, the interrogation spot size of 128 × 128 was required to compute correct vectors. The size of interrogation window was found to be the minimum size for accurate processing at the current concentration of the particles. This size was estimated by processing the images with interrogation window sizes varying from 32 × 32 pixels to 128 × 128 pixels and choosing the size that resulted minimum spurious vectors. The good quality images insured that very few wrong vectors were computed.

Results and Discussion

Contact angle and droplet height

When a liquid droplet undergoes evaporation the loss of vapor mass causes decrease in its volume. For a small droplet, the surface tension force will keep the shape spherical. If the substrate surface is smooth and nonwetting then the contact angle will not change but its radius will continuously decrease. On the other hand, for a droplet placed on a wetting and rough substrate the contact line gets pinned and as a result of evaporation loss the contact angle and height of the drop decreases continuously.[1] We have determined the contact angle from the recorded images and its time evolution is shown in the Figure 4. Uno et al.[35] have carried out experimental studies of particle adsorption in 3D evaporating droplets of latex dispersions on hydrophilic and hydrophobic surfaces. We have included for comparison their result for the time evolution of contact angle for 0.1% latex dispersion droplet on ordinary cover glass substrate similar to one used in the present work. In this plot, the contact angle θ is scaled by initial contact angle θ_o and evaporation time t is scaled by the total drying time t_d. The initial droplet contact angle in this case was observed to be 62°. We observe reasonably good agreement with their data suggesting that the evaporation dynamics in the disc-shaped 2D droplets is qualitatively similar to the 3D axi-symmetric sessile droplets. It is observed that the contact angle decreases almost linearly with time except in the beginning and later stages of the evaporation. In another experiment the evaporation was carried out under IR radiation. In this case also we observe that the decrease in contact angle with time is linear but the slope is steeper due to enhanced evaporation rate. Overall, there is good qualitative agreement with the 3D experiments indicating that the 2D configuration can have dynamic similarity with the 3D droplet. However, it is likely that the curvature of the confined drop will be different from that of 3D droplet evaporating in the ambient and hence the Marangoni number will also be different. For the same Marangoni number for the 2D and 3D flow the expected behavior should be similar. Besides Marangoni number, the evaporation flux from a sessile droplet depends on factors like undersaturation of vapor, contact angle, radius of the drop. However, it is not clear whether in general the transport in the vapor phase surrounding the droplet is diffusive or convective.[3] For convection dominated regime the evaporation rate should vary as the surface area of the drop. Hence, for 3D drop of radius R the evaporation rate will be much higher ($\sim R^2$) compared to the evaporation rate of the confined disc-shaped drop ($\sim Rh$) of same radius R and thickness h (where $h < R$) under similar conditions of evaporation.

The height of the droplet (Figure 5) also shows a similar linear behavior with dimensionless time ($t' = t/t_0$), where t_0 is the time at which the droplet showed no dispersed particles and this happened at contact angle of 24° for this case. As the shape of the drop always remains that of a partially circular disc, the mass m of the liquid drop of density ρ,

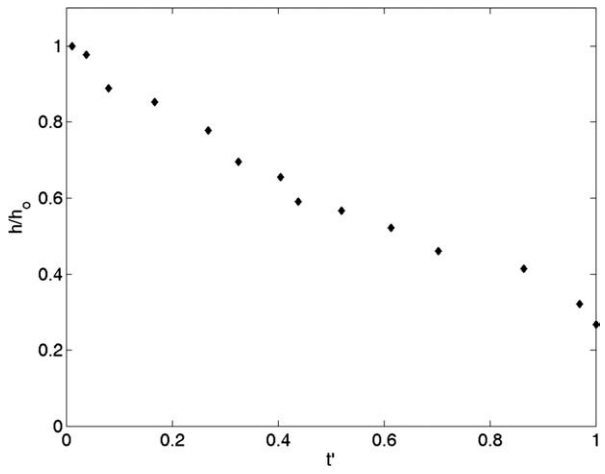

Figure 5. Variation of the height (h) normalized by the initial drop height (h_0) of the droplet with dimensionless evaporation time.

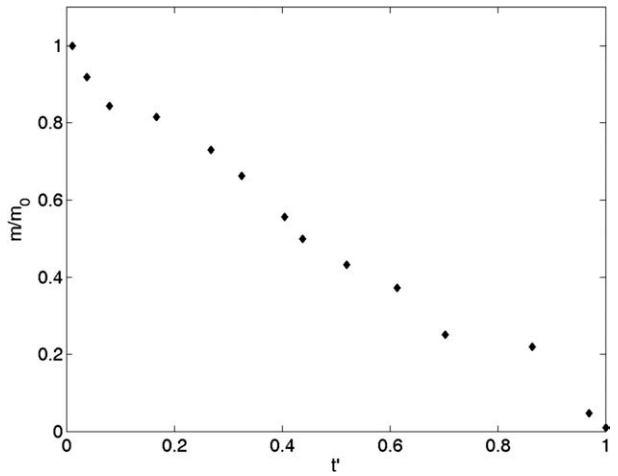

Figure 6. The mass (m) of the droplet normalized by the initial drop mass (m_0) plotted against the dimensionless evaporation time.

contact angle θ, height h, base radius R and thickness Δz can be calculated from $m = \rho[(R^2\theta - 0.5R(R - h)]\Delta z$. The change in the droplet mass with time is a measure of evaporation rate and is shown in Figure 6. In this work, we are unable to compare the evaporation flux between the confined droplet and the 3D sessile droplet as the droplet diameter and evaporation conditions can be quite different. We only speculate based on the plot of droplet mass with time in Figure 6 that the evaporation rate is grossly constant. By comparing the % decrease in volume of droplet with time we observed that the evaporation rate in our experiments was about 1.6 times lower than that of Uno et al.[35] for 3D sessile droplet. Here, we mention that the purpose of lateral confining surface was to make the disc-shaped drop but at the same time it should not offer any resistance to the receding drop. For this purpose, we have made these surfaces nonwetting and slippery by coating with paraffin wax. The smoothness of the data in the Figure 6 can be treated as measure of smoothness of the confining surfaces and continuous decrease of mass with time indicates that the lateral surfaces are not changing the droplet dynamics significantly. Any such inhomogeneity in the lateral confining surfaces would have produced irregular decline of the droplet volume, which is not observed here.

Velocity field

There is very little work done in the past to obtain quantitative information on the flow field inside an evaporating droplet. To our knowledge, the work by Kang et al.,[25] Pereira et al.,[27] and Ueno and Kochiya[28] are so far the only available sources providing such experimental information. The experimental work of Kang et al.[25] using the ray tracing method have determined the instantaneous velocity vector map of an evaporating droplet of ethanol-water mixture. For a similar system of ethanol-water droplet, Pereira et al.[27] have presented the time evolution of particle tracks using the defocusing digital particle tracking velocimetry (DDPTV). The faster evaporation of ethanol makes the fluid density at the droplet surface greater than the core region. This generates buoyancy induced convection besides the Marangoni convection due to the temperature gradients along the fluid interface. At low concentration of ethanol they observed a pair of counter rotating vortices with fluid moving upward in the central region. Hu and Lasron[10] have measured the flow field in the evaporating droplets using an out of focus particle tracking method. Their experiments with water drops show very weak Marangoni flow. However, their theoretical flow field for the same Marangoni number did not match with the experiments. This they have attributed to the presence of contaminants at the water surface which reduces the surface tension. Our experiments show that Marangoni convection cells are generated even within the evaporating pure water droplets (Figure 7) similar to the observations of Kang et al.[25] The velocity vectors show two counter-rotating vortices which are symmetric about the centre. Thus, it appears that the chance of surface contamination in our case is less due to small free surface area of the disc-shaped droplet, besides the confining lateral surfaces prevents such contamination. The convection cells observed in our experiments are mainly from the Marangoni flow due to the temperature gradient developed along the surface due to evaporation. The edge of the drop has highest evaporative heat loss and therefore it is at lower temperature than the apex. The surface tension decreases with the temperature and therefore this gradient will drive an anticlockwise flow in the left half and clockwise flow in the right half of the droplet. It can be observed that the fluid moves upward in the central region carrying the solute particles to the surface and then moves toward the edge along the free surface of the droplet. As the droplet is axi-symmetric, fluid in the central core moves upward along the axis, then return to the substrate plane along outer surface. In this process some of the particles are deposited at the edge. Figure 7b shows another vector plot at 1200 s of evaporation time when the contact angle has

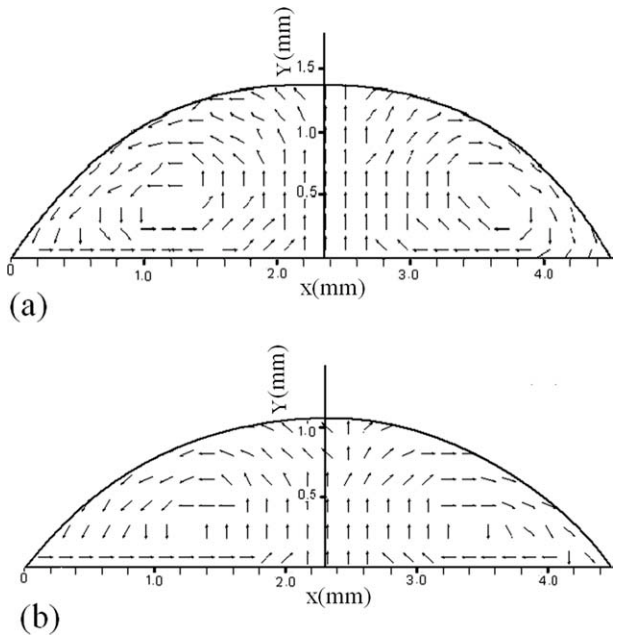

Figure 7. (a) Velocity field at 50 s and (b) at 1200 s of evaporation time; two counter-rotating vortices can be seen in these pictures.

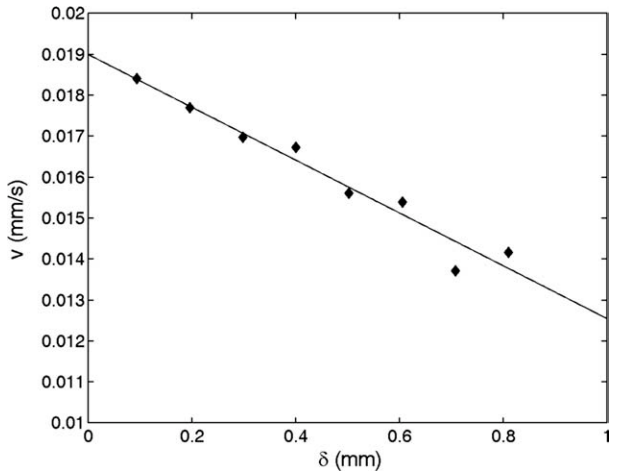

Figure 8. The height averaged radial velocity vs. the distance from the contact line, $\delta = R - r$.

The solid line is the best linear fit of the experimental data.

reduced to about 40°. When the contact angle decreased to low values there were few dispersed particles making the finding of correlation peaks erroneous and hence it was not possible to get enough velocity vectors at the current concentration of particles.

Hu and Larson[9] have obtained analytical and numerical solution of Marangoni flow field in an evaporating sessile droplet. The numerical simulations were performed for thermal Marangoni number defined as $Ma = -\beta\Delta T_o t_f/\mu R$, which is a ratio of Marangoni force to viscous force for a drop of viscosity μ and radius R. The temperature coefficient of surface tension of water is denoted by β, and ΔT_o is the temperature difference between the edge and top of the droplet whose total evaporation time is t_f. Thermal field in the droplet can change significantly with evaporation time and it can reverse the flow direction. In the case of full 3D droplet and at early time of evaporation, the longer conduction path from the bottom of the substrate to the top of the droplet makes the temperature lower at the top of the droplet than elsewhere, resulting a positive Marangoni number and hence a clockwise rotation in the left half and anticlockwise rotation in the right half of the droplet. They also observed that at longer times the faster rate of evaporation at the droplet edge makes it cooler there and there is reversal of recirculation direction below the contact angle of 14°. In our experiments on drop confined in the narrow gap between two surfaces, every point on the free surface has the same conduction path but the faster evaporation from the pinned edge causes there lower temperature compared to the apex of the drop. This produces negative Marangoni number and hence we observed clock-wise rotation in the right half of the droplet and anti-clockwise rotation in the left half. Similar velocity profiles were also observed for the experiments carried out in the presence of IR radiation.

The radial velocity near the pinned edge of the drop is responsible for the deposition of solute particles at the contact line. A radial outward flow will cause ring like deposition and an inward flow will make uniform deposition on the substrate upon drying. Deegan et al.[3] have theoretically shown that a nonzero velocity inside the drop arises when there is a mismatch between the local evaporation rate and the rate of change of interface height. The evaporation rate depends on whether the rate-limiting step is the transfer rate across the liquid-vapor interface or is the diffusive relaxation of the saturated vapor layer adjacent to the drop. In the former case, evaporation flux J_s is constant, while in the later case close to the contact line $J_s \sim (R - r)^{-\lambda}$, where $\lambda = (\pi - 2\theta)/(2\pi - 2\theta)$ and θ is the contact angle the liquid droplet of radius R makes with the substrate. They argue that at longer times the diffusive flux dominates and near the edge of the drop where the velocity contribution of change in height of interface is negligible, the vertically averaged radial velocity $v \sim (R - r)^{-\lambda}$. They have also conducted experiments with very small contact angle ($\theta = 15°$) and tracked the radial motion of the particles using fluorescent microscopy. At later stage of evaporation when the depth of the liquid became small ($\theta = 12°$, $\lambda = 0.47$), they measured the radial velocity in a region extending two-thirds of the way out from the centre of the drop up to the contact line. They observed reasonable agreement with the theoretical value of the velocity $v \sim (R - r)^{-\lambda}$. In Figure 8 we have plotted the height averaged velocity vs. distance from the contact line $\delta = R - r$, where R is the droplet radius and r is radial position measured from the centre of the droplet. The contact angle θ for this case was 40° and the corresponding value of λ was 0.35. We observe a linear behavior rather than the power law behavior. When the evaporation flux and the rate of change of interface height is constant, theoretical analysis of Deegan et al. predicts $v \sim r/h$, where h is the height of the interface at any radial location r. For a wedge-shaped region near the contact line, r/h decreases linearly with $(R - r)$. Thus, our result in the Figure 8 substantiates the analysis of Deegan et al. that in the early stages of evaporation, rate limiting step is the transfer rate across the liquid-vapor interface. We were unable to get velocity vectors in the later stages of evaporation when the contact angle decreased to low values.

Particle concentration

To evaluate the concentration of solute particles the droplet is divided into 10 bins of equal width as shown in Figure 9. The number of particles dispersed in each bin is counted using a particle tracking program. To get correct count of the dispersed particles it was necessary to remove the pixels forming the boundary of the drop. After importing the image, boundary of the area of interest is found by locating the free surface and solid surface. Free surface and solid

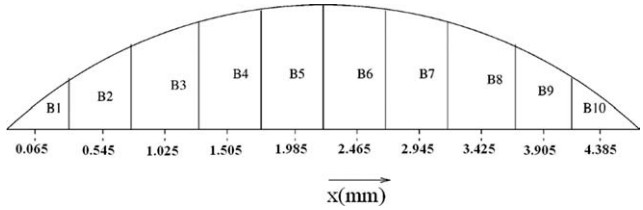

Figure 9. Schematic representation of bins in droplet used for the analysis of solute concentration.

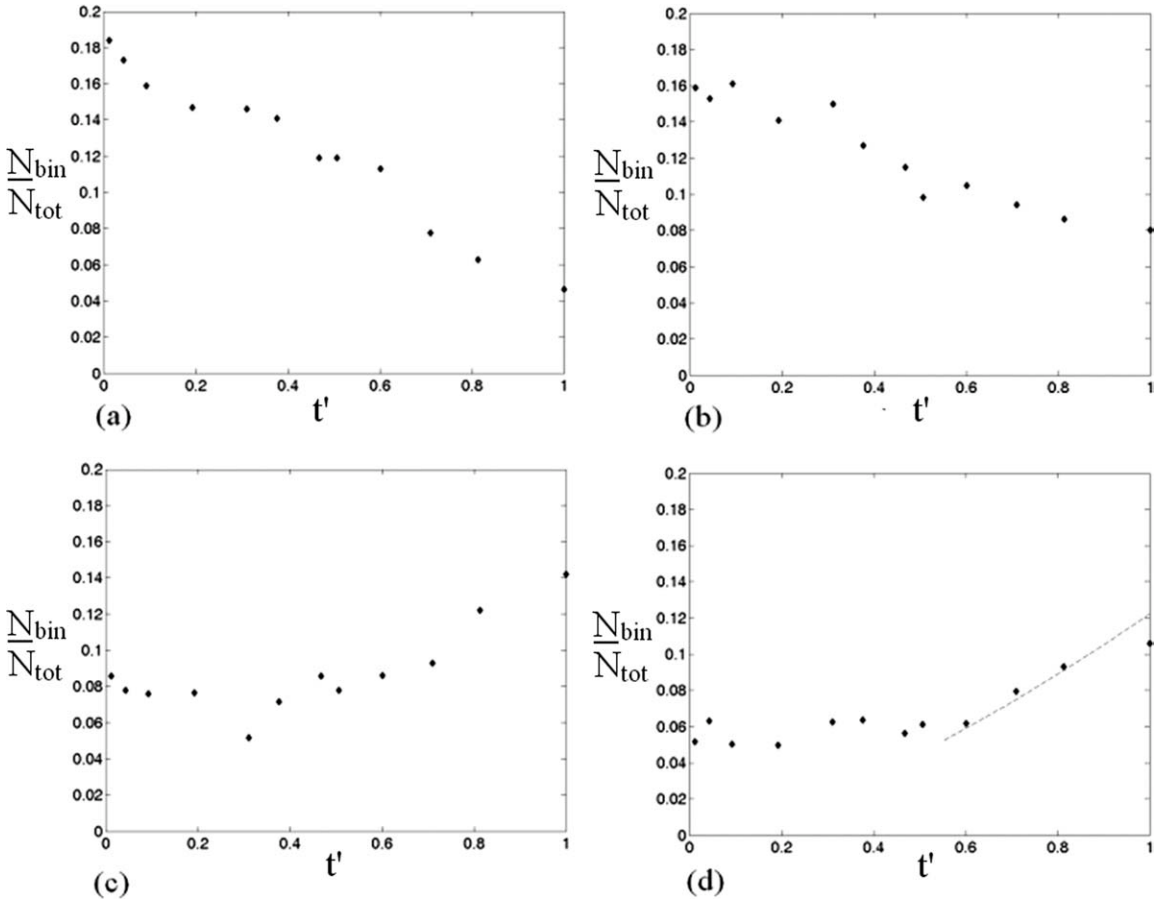

Figure 10. Particle concentration plotted vs. time at various radial positions: (a) bin 6 (b) bin 7 (c) bin 9 (d) bin 10.

The dashed line in the figure (d) is a fit to $N_{bin}/N_{tot} = a(t')^{1.43}$.

surface are shown in thick white region in the image (Figure 3a). Thick white region is determined as point above which the pixel intensity is continuously above 250. The cleaned image was shown in Figure 3b. In this cleaned image the intensity value ranged from 0 to 255. An average particle in the image frame was represented by 2 pixels. Hence, two adjacent pixels of intensity range in between 240 and 255 were counted as one particle. All the particles in the image frame were tagged and counted. This information was subsequently used to determine the particle concentration inside the droplet. It is likely that there are particle overlaps and the present algorithm was not able to distinguish them. This may introduce small error in the particle count but it is not expected to alter the result qualitatively.

The dispersed particle concentration (N_{bin}/N_{tot}) denotes the number of particles dispersed at any instant in a bin divided by the total particles present initially in the whole droplet. To obtain the particle concentration value at a given time a set of 100 images was analyzed to get an average count. This amounts to averaging over a period of 5 s. Figure 10 shows the dispersed particle concentration in different bins. We can see from Figures 10a, b that the particle concentrations in bin 6 and 7 which are near the central region of the droplet decreases continuously with time. Similar trend was also observed in the bins on the left half (not shown here) of the droplet. On the other hand, we see that the particle concentration in the bins close to the edge increases (See Figures 10c, d). The scatter in particle concentration data could be due to the fact that due to rotating vortices, the number of particle in a bin is changing over time. An average over long time may reduce the scatter, but the averaging

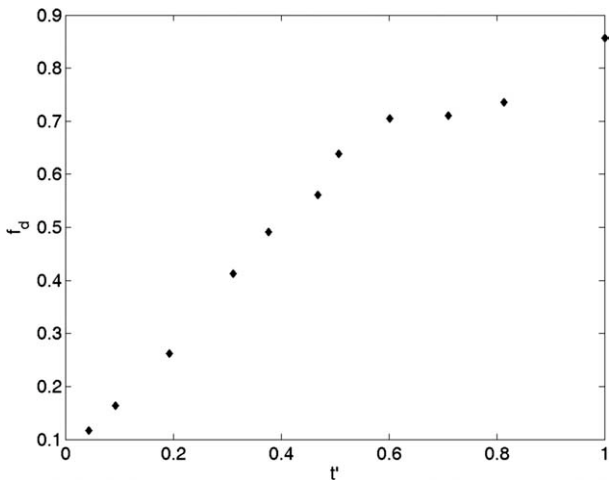

Figure 11. Fraction of the deposited particles plotted vs. dimensionless time.

time taken should be small enough for any significant change in the droplet height. There is also a possibility of out of plane motion in the normal direction which can be reduced by decreasing the thickness of the droplet disc. The growth of the particle in the last bin (Figure 10d) gives a measure of the ring mass throughout the drying time. We observe slow growth at early times followed by a late time surge in the growth rate. We observe that the late time surge closely follows the theoretical prediction of Deegan et al.[3] which says that the growth in the deposited particle varies as $m_R \sim t^{2/(1+\lambda)}$. As λ changes with the evaporation time, we have used the average value of 0.39 toward the later half of the evaporation when the contact angle varied from 40° to 24°. This suggests that one should expect that the number of deposited particles should grow as $t^{2/(1+0.39)} \approx t^{1.43}$. The dashed line in the Figure 10d is a fit to the curve $N_{bin}/N_{tot} = a(t')^{1.43}$. Deegan et al. have also presented experimental count of total number of particles arriving at the contact line. The initial contact angle at the start of count in their experiment was 15°. Their experimental values are in good agreement with the theory for the early stages of the evaporation but considerably higher over the theoretical prediction for the late-time surge behavior. It is to be noted from Figure 10d that in the early stages of evaporation the particles remain dispersed in the droplet due to strong recirculating flow. Significant deposition only starts when the contact angle decreases to low values and the radially outward flow dominates. The Figure 11 shows the variation of fraction of initial particles deposited with time. The deposited particles at a given instant was calculated by subtracting the number of dispersed particles from initial count of dispersed particles in the drop. It can be seen that in an evaporating droplet the flow can carry most of the particle towards the edge, and the ring mass grows with time. During the early stage of evaporation when the contact angle decreases from 62° to 40°, it can be observed that close to 70% particles have been deposited and by the time the contact angle has become 24° almost 87% of particles have been deposited. Beyond the contact angle of 24° our particle tracking algorithm could not detect any particle in the bins. It is also likely that a small amount of particles accumulating near the free surface are not contributing to the growth of edge deposition. However, it is expected that due to strong Marangoni convection such particles are pulled inwards towards the edge or circulate back in the bulk. There is also a possibility of out of plane motion and likelihood of some particles not showing intense images and missing out in the particle count. This can be reduced by illuminating the droplet with a thin laser sheet. We also had tried a laser sheet illumination but strong scattering of laser light from the droplet free surface and glass substrate resulted into unwanted illuminations. Overall, the aforementioned factors can change the particle count from time to time and appear as noise in the observed data but it should not change the result qualitatively.

Conclusions

We have carried out simple flow visualization experiments in an evaporating droplet containing solute particles. The 2D visualization of a drop confined in the narrow gap between the two parallel transparent surfaces ensured good images in the velocity plane which was analyzed using the technique of particle image velocimetry to get velocity vectors. As the image plane and flow field were perpendicular to the camera, no velocity or image mapping was required. From the PIV analysis, we observe that two symmetric counter-rotating vortices are present. As the evaporation progresses the contact angle and height of the droplet continuously decreases. We have also measured the particle concentration at various times during the evaporation process. The particle concentration in the central portion of the drop decreases with time whereas it increases towards the edge leading to ring-like deposits. Thus, it has been observed that the evaporation induced forces driving the particles from the middle of the drop to the edge are responsible for particle transport and ring formation in drying droplets. It is true that many droplet internal circulation flows have 3D characteristics and require capture of 3D features and in such cases 3D PIV or PTV method will be desirable. If one is interested in issues related to the flow instabilities under different conditions of evaporation then it would require fully three-dimensional flow mapping and the present technique of 2D drop may not be useful. The 2D problem cannot be used to visualize vortex flow in those planes which are not perpendicular to the base. Nevertheless our concept extends to any symmetrically evaporating droplet where the knowledge of time-resolved planar velocity and concentration field is required. The contact surface need not be transparent and this can be applied to any type of surface. An additional advantage of this method is that the flow field can be mapped for nontransparent droplets using fluorescent tracers.

Acknowledgments

The authors acknowledge funding from the Department of Science and Technology through the project no. SR/CE/38/06.

Literature Cited

1. Deegan RD, Bakajin O, Dupont TF, Huber G, Nagel SR, Witten TA. Capillary flow as the cause of ring stains from dried liquid drops. *Nature*. 1997;389:827–829.
2. Deegan RD. Pattern formation in drying drops. *Phys Rev E*. 2000; 61:475–485.
3. Deegan RD, Bakajin O, Dupont TF, Huber G, Nagel SR, Witten TA. Contact line deposit in an evaporating drop. *Phys Rev E*. 2000;62:756–765.
4. Popov YO. Evaporative deposition patterns: spatial dimension of the deposit. *Phys Rev E*. 2005;71:036313-1–036313-17.
5. Fischer BJ. Particle convection in an evaporating colloidal droplet. *Langmuir*. 2002;18:60–67.
6. Widjaja E, Harris MT. Particle deposition study during sessile drop evaporation. *AIChE J*. 2008;54:2250–2260.
7. Hu H, Larson RG. Evaporation of a sessile droplet on a substrate. *J Phys Chem B*. 2002;106:1334–1344.
8. Hu H, Larson RG. Analysis of the microfluid flow in an evaporating sessile droplet. *Langmuir*. 2005;21:3963–3971.
9. Hu H, Larson RG. Analysis of the effects of Marangoni stresses on the microflow in an evaporating sessile droplet. *Langmuir*. 2005; 21:3972–3980.
10. Hu H, Larson RG. Marangoni effect reverses coffee-ring depositions. *J Phys Chem B*. 2006;110:7090–7094.
11. Pearson JRA. On convetion cells induced by surface tension. *J Fluid Mech*. 1958;4:489–500.
12. Nguyen VX, Stebe KJ. Patterning of small particles by a surfactant-enhanced Marangoni-Benard instability. *Phys Rev Lett*. 2002;88: 164501–164501-4.

13. Adachi E, Dimitrov AS, Nagayama K. Stripe patterns formed on a glass surface during droplet evaporation. *Langmuir*. 1995;11:1057–1060.
14. Yabu H, Shimomura M. Preparation of self-organized mesoscale polymer patterns on a solid substrate: continuous pattern formation from a receding meniscus. *Adv Funct Mater*. 2005;15:575–581.
15. Hong SW, Xu J, Xia J, Lin Z, Qui F, Yang Y. Drying mediated pattern formation in a capillary-held organometallic polymer solution. *Chem Mater*. 2005;17:6223–6226.
16. Abkarian M, Nunes J, Stone HA. Colloidal crystallization and banding in a cylindrical geometry. *J Am Chem Soc*. 2004;126:5978–5979.
17. Lin Z, Granick S. Patterns formed by droplet evaporation from a restricted geometry. *J Am Chem Soc*. 2005;127:2816–2817.
18. Xu J, Xia J, Hong SW, Lin Z, Qiu F, Yang Y. Self-assembly of gradient concentric rings via solvent evaporation from a capillary bridge. *Phys Rev Lett*. 2006;96:066104-1–066104-4.
19. Xu J, Xia J, Lin Z. Evaporation-induced self-assembly of nanoparticles from a sphere-on-flat geometry. *Angew Chem Int Ed*. 2007; 46:1860–1863.
20. Byun M, Laskowski RL, He M, Qui F, Jeffries-EL M, Lin Z. Controlled evaporative self-assembly of hierarchically structured regioregular conjugated polymers. *Soft Matter*. 2009;5:1583–1586.
21. Hong SW, Xia J, Lin Z. Spontaneous formation of mesoscale polymer patterns in an evaporating bound solution. *Adv Mater*. 2007; 19:1413–1417.
22. Hong SW, Byun M, Lin Z. Robust self-assembly of highly ordered complex structures by controlled evaporation of confined microfluidics. *Angew Chem Int Ed*. 2009;48:512–516.
23. Zhang N, Wang WJ. Natural convection in evaporating minute drops. *J Heat Transfer*. 1982;104:656–662.
24. Savino R, Monti R. Buoyancy and surface-tension driven convection in hanging drop protein crystallizer. *J Cryst Growth*. 1996;165:308–318.
25. Kang KH, Lee SJ, Lee CM, Kang S. Quantitative visualization of flow inside an evaporating droplet using the ray tracing method. *Meas Sci Technol*. 2004;15:1104–1112.
26. Minor G, Oshkai P, Djilali N. Optical distortion correction for liquid droplet visualization using the ray tracing method: further considerations. *Meas Sci Technol*. 2007;18:23–28.
27. Pereira F, Lu J, Castano-Graff E, Gharib M. Microscale 3D flow mapping with μDDPIV. *Exp Fluids*. 2007;42:589–599.
28. Ueno I, Kochiya K. Effect of evaporation and solutocapillary-driven flow upon motion and resultant deposition of suspensded particles in volatile droplet on solid substrate. *Adv Space Res*. 2008;41:2089–2093.
29. Abramchuk SS, Khokhlov AR, Iwataki T, Oana H, Yoshikawa K, Direct observation of DNA molecules in a convection flow of a drying droplet. *Europhys Lett*. 2001;55:294–300.
30. Chopra M, Li L, Hu H, Burns MA, Larson RG. DNA molecular configuration in an evaporating droplet near a glass surface. *J Rheol*. 2003;47:1111–1132.
31. Denkov ND, Velev OD, Kralchevsky PA, Ivanov IB, Yoshimura H, Nagayama K. Mechanism of formation of two-dimensional crystals from latex particles on substrates. *Langmuir*. 1992;8:3183–3190.
32. Dimitrov AS, Dushkin CD, Yoshimura H, Nagayama K. Observations of latex particle two-dimensional-crystal nucleation in wetting films on mercury, glass, and mica. *Langmuir*. 1994;10:432–440.
33. Adrian RJ, Keane RD, Zhang Y. Super resolution particle imaging velocimetry. *Meas Sci Technol*. 1995;6:754–768.
34. Christensen KT, Soloff SM, Adrian RJ. PIV Sleuth: integrated particle image velocimetry interrogation/validation software. Technical Report, Department of Theoretical and Applied Mechanics, University of Illinois at Urbana-Champaign, 2000.
35. Uno K, Hayashi K, Hayashi T, Ito K, Kitano H. Particle adsorption in evaporating droplets of polymer latex dispersions on hydrophilic and hydrophobic surfaces. *Colloid Polym Sci*. 1998;276: 810–815.

Manuscript received Apr. 9, 2009, and revision received Sept. 12, 2009.